First Imaging Experiment of a Lithium Ion Battery by a Pulsed Neutron Beam at J-PARC/MLF/BL09

AUTHOR(S):

Kino, Koichi; Yonemura, Masao; Kiyanagi, Yoshiaki; Ishikawa, Yoshihisa; Parker, Joseph. Don.; Tanimori, Toru; Kamiyama, Takashi

CITATION:

Kino, Koichi ...[et al]. First Imaging Experiment of a Lithium Ion Battery by a Pulsed Neutron Beam at J-PARC/MLF/BL09. Physics Procedia 2015, 69: 612-618

ISSUE DATE:

2015

URL:

http://hdl.handle.net/2433/226434

Available online at www.sciencedirect.com

ScienceDirect

Physics Procedia 69 (2015) 612 – 618

Physics Procedia

10 World Conference on Neutron Radiography 5-10 October 2014

First Imaging Experiment of a Lithium Ion Battery by a Pulsed Neutron Beam at J-PARC/MLF/BL09

Koichi Kino[a,*], Masao Yonemura[b], Yoshiaki Kiyanagi[a,c], Yoshihisa Ishikawa[b], Joseph. Don. Parker[d,e], Toru Tanimori[d], Takashi Kamiyama[b]

[a]*Faculty of Engineering, Hokkaido University, N-13 W-8 Kita-ku, Sapporo 060-8628, Japan*
[b]*IMSS, High Energy Accelerator Research Organization, 1-1 Oho, Tsukuba Ibaraki 305-0801, Japan*
[c]*Graduate School of Engineering, Nagoya University, Furo-cho Chikusa-ku, Nagoya 464-8603, Japan*
[d]*Department of Physics, Kyoto University, Kitashirakawa-oiwakecho Sakyo-ku, Kyoto 606-8502, Japan*
[e]*Research Center for Neutron Science and Technology, Comprehensive Research Organization for Science and Society, 162-1 Shirakata Tokai, Ibaraki 319-1106, Japan*

Abstract

We obtain the transmission image of a commercial lithium ion (Li-ion) battery using a pulsed neutron beam at the beamline 09 of the Materials and Life Science Experimental Facility at the Japan Proton Accelerator Research Complex. The purpose of this study is to improve the performance of the Li-ion battery by nondestructive observation of its charging and discharging. The transmission images for three charge states (3.2 V, 3.7 V, and 4.2 V) reveal differences between these three states, which we attribute to electrolyte migration. The transmission spectra show Bragg edges originating from the electrodes, current collectors, and battery vessel. Although the battery as a whole has the expected relation between the charge accumulation and the quantity of lithium amounts in the positive and negative electrodes, a portion of the battery deviates from this relation, which may imply a position dependent charging in the battery.

Selection and peer-review under responsibility of Paul Scherrer Institut

Keywords: Imaging; Pulsed neutron beam; Li-ion battery; J-PARC; BL09;

* Corresponding author. Tel.: +81-11-706-6703; fax: +81-11-706-6703.
*E-mail address:*k-kino@eng.hokudai.ac.jp

Selection and peer-review under responsibility of Paul Scherrer Institut
doi:10.1016/j.phpro.2015.07.087

1. Introduction

For iron and steel, the crystalline phase, texture, and strain have been imaged by detecting Bragg edges with a wavelength-selected neutron beam and a two-dimensional neutron detector. Santisteban et al. (2002), Sato et al. (2011), Woracek et al. (2011), Woracek et al. (2014) This technique can be applied to other crystalline materials and the Li-ion battery is an attractive material. The reason is that the Li-ion battery charges and discharges by the intercalation and deintercalation of Li ions between the crystalline materials of the positive and negative electrodes. Detecting Bragg edges allows us to monitor the crystalline structure and lattice parameter, thereby providing nondestructive technique to image the charged and discharged states of a Li-ion battery. In fact, the Bragg edge of the negative electrode (graphite) and its change during discharge has been reported using a monochromatic neutron beam at the FRM II reactor. Butler et al. (2011) However, detecting Bragg edges over a wide range of neutron wavelengths is difficult to do by changing the wavelength of a monochromatic neutron beam. Therefore, in the present study, we use an intense pulsed neutron beam to detect Bragg edges with multiple Miller indices for both the positive- and negative-electrode materials of a Li-ion battery.

The study of Li-ion battery by the powder diffraction method has been already performed using intense neutron beam, such as from a nuclear reactor or pulsed neutron source. Sharma et al. (2010), Senyshyn et al. (2012), Wang et al. (2012), Yonemura et al. (2014) In particular, using the VULCAN beamline at the Spallation Neutron Source at Oak Ridge National Laboratory, the position dependence-deterioration of a Li-ion battery was determined by scanning the sample through a narrow neutron beam. Cai et al. (2013) However, this experiment did not reveal the quantity of intercalation and deintercalation of Li ion. In contrast, the transmission method, which we use, can provide quantitative images of charge and discharge states because the depth of the Bragg edges corresponds to the quantity of crystals: in other words, the numbers per unit area of Li-ions in the positive and negative electrodes. This property of the transmission method for the Li-ion battery makes it useful for quantitatively studying the position dependence of charging and discharging in a Li-ion battery. Nonuniformity in the charging and discharging of a Li-ion battery could occur due to a nonuniformity of the conductive auxiliary on the current collectors and/or to a deterioration of the electrodes after the cycling of charging and discharging. Therefore, the goal of the present study is to detect any position dependent charging and discharging, with the final goal being to improve the power density and cycle property of Li-ion batteries.

2. Experiment

We used beamline 09 (BL09) Yonemura et al. (2014) at the Materials and Life Science Experimental Facility at the Japan Proton Accelerator Research Complex. BL09 was constructed for studying batteries using neutron powder diffraction. A high $\Delta d/d$ resolution of 0.09% is available by using a neutron source with a decoupled-poisoned moderator neutron source and a 52-m flight path between the neutron source and sample. BL09 is equipped with a neutron powder diffractometer called SPICA, which mainly comprises a sample chamber with backscattering, 90°, and low-angle detector banks.

We used a micro-pixel chamber-type (μPIC-type) two-dimensional neutron detector Parker et al. (2013), which mainly comprises a gas chamber and μPIC. Mixed gas of argon, ethane, and helium-3 ($Ar:C_2H_6:He\text{-}3 = 66:7:30$) at 2 atmosphere and detection depth of 25 mm is filled in the gas chamber made of aluminum. If a neutron enters the gas chamber and reacts with He-3, a proton and triton are emitted in opposite directions. The electrons liberated by ionization along the tracks of these two particles drift to the μPIC due to an electric field imposed in the gas chamber, and the incident time and two-dimensional position are recorded. The spatial resolution of the detector is ~100 μm (one standard deviation), and the temporal resolution is ~1 μs. Its neutron-detection efficiency is 18% for neutron energy of 25.3 meV. The active area is 100×100 mm^2.

We used a commercial Li-ion battery as sample. This battery is cylindrical, 18 mm in diameter, and 65 mm in height. The battery was unused before the experiment and was positioned 100 mm upstream of the neutron detector. The experimental system, which comprises the sample and detector, was set in the sample chamber of the SPICA diffractometer.

The proton-beam power of the Japan Spallation Neutron Source was 218 kW. To avoid overflowing the neutron counter in the neutron detector, the neutron flux entering the neutron detector was reduced using a slit, which was

set between the end of the flight path and the battery. The maximum neutron-counting rate was 220 kcps. The disk chopper operated at 6.25 Hz, and the maximum neutron wavelength was 1.2 nm. We collected data with no sample for 9.4 h. The three data sets were collected over 14.3 h, 14.8 h, and 28.7 h with the battery in place at 3.2 V, 3.7 V, 4.2 V, respectively. Hereinafter, we refer to these three states of the battery as discharged, intermediate, and charged. Initially, charging was conducted in constant-current mode (0.5 A) until the voltage reach 3.7 V or 4.2 V, after which it was switched to the constant-voltage mode. Charging ended when the current dropped to 60 mA.

3. Analysis and Discussion

Fig. 1 shows transmission images of the three states of the Li-ion battery acquired with a neutron wavelength from 0.1 to 0.8 nm. These are images from incoming neutron beam perspective, with the positive battery terminal at the bottom. The data between −6 and −3 mm are not shown because the corresponding channels of the neutron detector were broken. The figure shows that the transmission is very low in the central region of the sample, which is attributed to neutron absorption by Li-6 and neutron scattering from H in the battery. This low transmission increases slightly throughout the vertical length of the battery from −1 to +1 mm in the horizontal direction, which is due to the structure of the cylindrical shape of the battery, wherein layers of the positive and negative electrodes and separator are rolled, leaving a void in the center due to the large curvature.

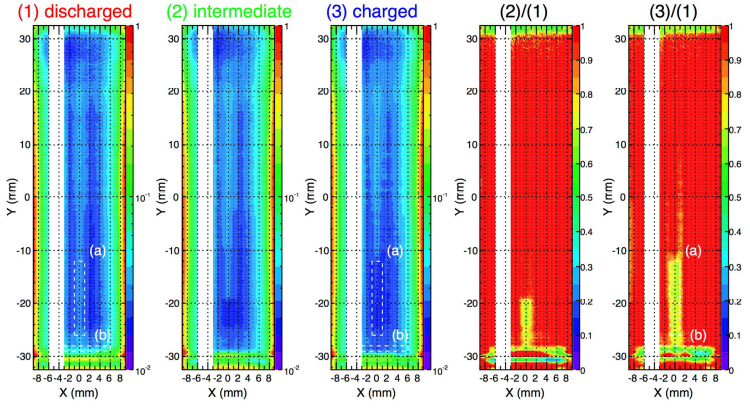

Fig. 1. Transmission images of the three states of the battery obtained with a neutron wavelength from 0.1 to 0.8 nm. The positive terminal is at the bottom in these images. The range from X = −6 to −3 mm is not shown because the neutron-detector channels were broken in this range. The two panels on the right side show the ratios of the images of the intermediate-to-discharged [(2)/(1)] and charged-to-discharged [(3)/(1)] states.

The transmission images of the three states differ, as shown clearly by the panels on the right side of Fig. 1, which, going from left to right, show the ratios of the images of the intermediate to discharged states and of the charged to discharged states (as indicated above each panel). To facilitate further analysis we define the areas (a) and (b) by the dashed rectangles. Fig. 2(a) and 2(b) show the transmission spectra for the discharged and charged states of areas (a) and (b), respectively. For almost the entire wavelength range studied and for both areas, the transmission of the charged state is less than that of the discharged state. The ratio of the transmission of the charged state to discharged state is shown in Fig. 2(c) and 2(d) for areas (a) and (b), respectively. The ratio decreases gradually with increasing wavelength. The materials that can migrate in the Li-ion battery are electrolyte and Li. Ethylene (CH_2), which is a component of most electrolytes, strongly scatters neutrons, and ethylene carbonate (EC), which is a typical electrolyte, has two CH_2 in each molecule. The stable isotope Li-6 strongly absorbs neutrons. The pink and green curves in Fig. 2(c) and 2(d) are fits to the experimental spectra based on the neutron wavelength dependences of the total cross sections of CH_2 Lavelle et al. (2013) and Li-6, respectively. The pink fits reproduce the data much better than do the green fits. Therefore, we attribute the change in transmission in the areas (a) and (b) to the migration of electrolyte. Furthermore, assuming EC, we estimate the thickness of the

electrolyte from the fits in Fig. 2(c) and 2(d) to be 1.4 and 1.7 mm for areas (a) and (b), respectively. These values are not inconsistent with the size of the battery.

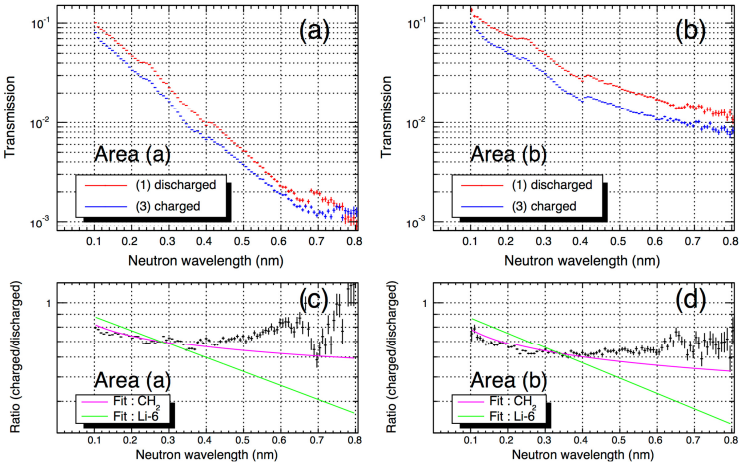

Fig. 2. Spectra of the transmission and ratio of transmission through areas labeled (a) and (b) in Fig. 1. (a) and (b) show the transmission spectra of the discharged and charged states, respectively. (c) and (d) show the ratio of the charged spectrum to the discharged spectrum for areas labeled (a) and (b), respectively, in Fig. 1. The pink and green curves are the fits based on the total cross sections of CH_2 and Li-6, respectively.

Fig. 3 shows transmission spectra of the three states. Many Bragg edges appear in the transmission spectra, which decrease exponentially with increasing neutron wavelength. Some Bragg edges depend on the charge state of the battery.

Fig. 4 shows the transmission spectra from 0.6 to 0.8 nm. The Bragg edge of graphite, which is the negative-electrode material, changes to that of LiC_{12} during the transition from the discharged to the intermediate state, and then changes to that of LiC_6 in the charged state. This change is attributed to the intercalation of Li ions. Fig. 5 shows the transmission spectra from 0.3 to 0.5 nm. The Bragg edges in this figure are assigned as indicated in the figure to the positive electrode ($Li_xNi_{0.8}Co_{0.2}O_2$), negative electrode (graphite, LiC_{12}, and LiC_6), current collector (copper and aluminum), and vessel (iron). Although the Bragg edges of the positive and negative electrodes change as expected depending on the charge state of the battery, the Bragg edges of other materials do not change as expected.

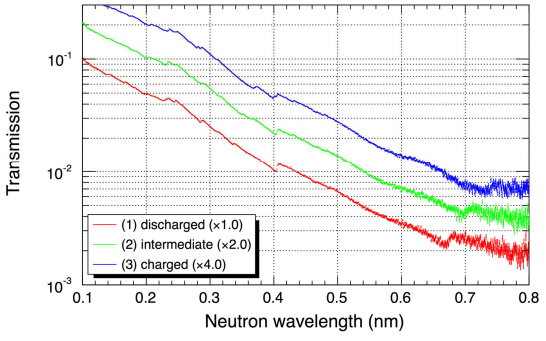

Fig. 3. The transmission spectra of three charge states of the battery

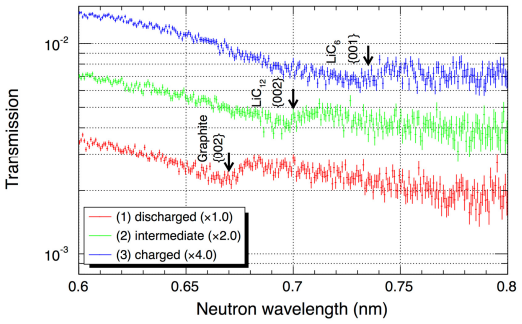

Fig. 4. Transmission spectra of three states of the battery as a function of neutron wavelength between 0.6 and 0.8 nm. The arrows indicate the wavelengths of the Bragg edges for graphite {002}, LiC_{12} {002}, and LiC_6 {001}.

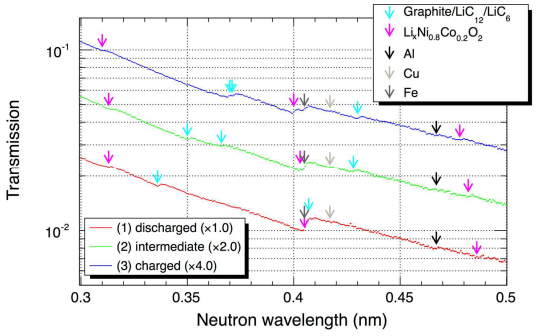

Fig. 5. Transmission spectra of three states of the battery as a function of neutron wavelength between 0.3 and 0.5 nm. The arrows indicate the wavelengths of the Bragg edges for materials of electrodes, current collectors, and battery vessel.

We fit the isolated Bragg edges of the positive and negative electrodes to a function describing the transmission spectrum expected from the coherent elastic cross section corresponding to the sum of the given Bragg edge, the neutron absorption cross section by Li-6, and a constant. This constant term serves to approximate the coherent elastic cross section of the other materials. The depth of the Bragg edges represents the quantity of crystalline material in the positive and negative electrodes per unit area. Therefore, we are able to ascertain the Li amount in the crystals.

Initially, we studied the area enclosed by the red rectangle in Fig. 6(a). We averaged the quantity of Li indicated by the Bragg edges from different Miller indices for the positive and negative electrodes. Fig. 7(a) shows the areal density of Li in the positive and negative electrode materials as a function of the accumulated charge during charging. For the discharged, intermediate, and charged states of $Li_xNi_{0.8}Co_{0.2}O_2$, we assumed the x=0.0, 0.5, and 1.0 in, respectively. Furthermore, we assumed zero Li in the negative-electrode material for the discharged state and in the positive- electrode material for the charged state. The quantity of Li in the negative- and positive-electrode materials is proportional and inversely proportional to the quantity of charge, which is reasonable considering the charging mechanism of the Li-ion battery.

Finally, we repeated the same analysis for the four areas shown in Fig. 6(b), and results are shown in Fig. 7(b). Three of the four areas exhibit a trend similar to that seen in Fig. 7(a). However, center-top area yields different results, which implies that battery-charging process depends on position. However, a better statistics is needed to confirm this conclusion.

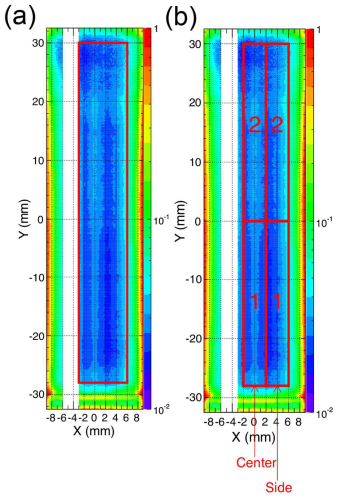

Fig. 6. Red rectangles show the areas of the battery where we analyzed the relation between the charge accumulated during charging and the quantity of Li in the electrode materials.

4. Conclusion and Future prospects

We acquired transmission images of a commercial Li-ion battery as a function of neutron wavelength using the pulsed neutron beam and two-dimensional neutron detector at J-PARC/MLF/BL09. In the wavelength range from 0.1 to 0.8 nm, part of the transmission images changed depending on the charge state of the battery. A detailed analysis that considers the neutron wavelength suggests the migration of electrolyte. The transmission spectra reveal Bragg edges, some of which depend on the intercalation and deintercalation of Li ions between the positive and negative electrodes. From the depth of the Bragg edges, we estimated the amount of Li in both electrode materials. In a large fraction of the cross section of the battery, the quantity of Li in the negative and positive electrodes is proportional and inversely proportional, respectively, to the charge accumulated during charging. This result is quite reasonable because Li ions move between the positive and negative electrodes that are typically 50 μm apart from each other. However, quarter of the total battery cross section affords different results, but a better statistics is needed to conclusively determine the position dependence of the charging.

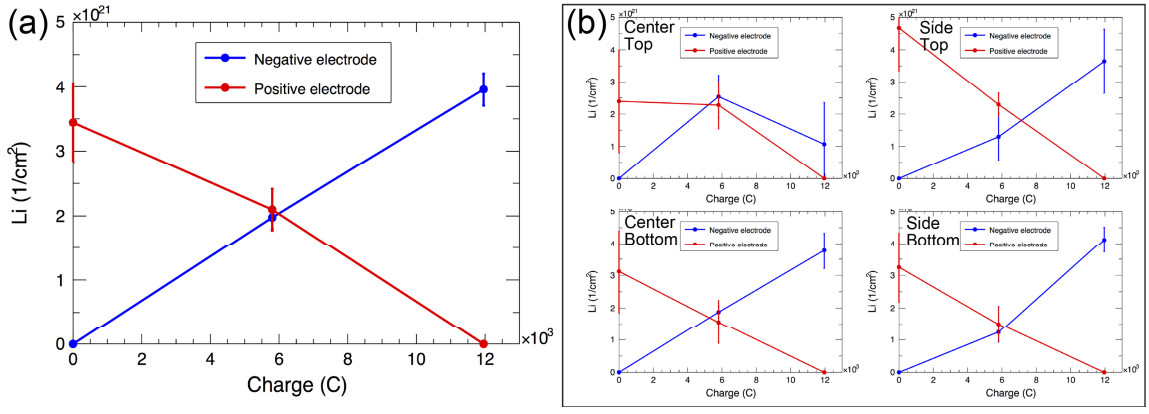

Fig. 7. (a) Quantity of Li in electrode materials as a function of the charge accumulated during charging for the area shown in Fig. 6(a). (b) Same as panel (a) but for the areas shown in Fig. 6(b).

Two improvements are expected to lead to a better statistics. The first is a new device that reduces the neutron-beam flux without changing the neutron-wavelength spectrum. Constructing transmission spectra requires data acquired with no sample in place in addition to data acquired with a sample in place. Because of the limitation in counting rate, we currently reduce the neutron-beam flux by narrowing the slits before the sample position to take measurements with no sample. However, the neutron-detector counting rate with no sample in place (i.e., the battery) is about one-tenth of that without the sample because the incident neutrons are scattered and absorbed by the battery. However, opening the slits would change the neutron-wavelength spectrum. This problem should be ameliorated when we install the new device, which will reduce the neutron-beam flux by a factor of ten for measurements without the sample in place can be made with ten times greater flux than is currently the case. This approach should give an order of magnitude better statistics. The second improvement is to upgrade the neutron detector to obtain a higher counting rate. Analog signals from the μPIC are digitized and transferred to a computer by Ethernet. At present, the maximum transfer rate is 100 Mbps. We will introduce revised electronics that allow 1 Gbps data transfer, which should also contribute a tenfold improvement in statistics. By combining these two improvements, we expect to acquire data in the near future with two orders of magnitude better than the data reported herein.

Acknowledgements

This study was partly supported by New Energy and Industrial Technology Development Organization (NEDO). This work was carried out as the S-type project of KEK (Proposal No. 2009S10, 2014S10).

References

Butler, G, L., et al., 2011. Neutron imaging of a commercial Li-ion battery during discharge: Application of monochromatic imaging and polychromatic dynamic tomography. Nuclear Instruments and Methods in Physics Research A 651, 320-328.

Cai, L., et al., 2013. In-situ observation of inhomogeneous degradation in large format Li-ion cells by neutron diffraction. Journal of Power Sources 236, 163-168.

Lavelle, M, C., Liu, Y, C., Stone, B, M., 2013. Toward a new polyethylene scattering law determined using inelastic neutron scattering. Nuclear Instruments and Methods in Physics Research A 711, 166-179.

Parker, D, J., et al., 2013. Spatial resolution of a μPIC–based neutron imaging detector. Nuclear Instruments and Methods in Physics Research A 726, 155-161.

Santisteban, J, R., et al., 2002. Strain imaging by Bragg edge neutron transmission. Nuclear Instruments and Methods in Physics Research A 481, 765-768.

Sato, H., Kamiyama, T., Kiyanagi, Y., 2011. A Rietveld-Type Analysis Code for Pulsed Neutron Bragg-Edge Transmission Imaging and Quantitative Evaluation of Texture and Microstructure of a Welded α-Iron Plate. Materials Transactions 52, 1294-1302.

Senyshyn, A., et al., 2012. “In-operando” neutron scattering studies on Li-ion batteries. Journal of Power Sources 203, 126-129.

Sharma, N., et al., 2010. Structural changes in a commercial lithium-ion battery during electrochemical cycling: An in situ neutron diffraction study. Journal of Power Sources 195, 8258-8266.

Wang, Xun-Li., et al., 2012. Visualizing the chemistry and structure dynamics in lithium-ion batteries by in-situ neutron diffraction. Nature Scientific Reports 2, 747.

Woracek, R., et al., 2011. Neutron Bragg-edge-imaging for strain mapping under in situ tensile loading. Journal of Applied Physics 109, 093506.

Woracek, R., et al., 2014. 3D Mapping of Crystallographic Phase Distribution using Energy-Selective Neutron Tomography. Advanced Materials 26, 4069-4073.

Yonemura, M., et al., 2014. Development of SPICA, New Dedicated Neutron Powder Diffractometer for Battery Studies. Journal of Physics: Conference Series 502, 012053.